

AJ, in press

Photometric Identification of Cool White Dwarfs¹

M. Kilic^{2,3}, D. E. Winget and Ted von Hippel

*The University of Texas at Austin, Department of Astronomy, 1 University Station C1400,
Austin, TX 78712, USA*

`kilic@, dew@, ted@astro.as.utexas.edu`

and

C. F. Claver⁴

*Kitt Peak National Observatory, National Optical Astronomy Observatory, P.O. Box
26732, Tucson, AZ 85726, USA*

`cclaver@noao.edu`

ABSTRACT

We investigate the use of a narrow-band DDO51 filter for photometric identification of cool white dwarfs. We report photometric observations of 30 known cool white dwarfs with temperatures ranging from 10,000 K down to very cool temperatures (≤ 3500 K). Follow-up spectroscopic observations of a sample of objects selected using this filter and our photometric observations show that DDO51 filter photometry can help select cool white dwarf candidates for follow-up multi-object spectroscopy by rejecting 65 % of main sequence stars with the

²Visiting Astronomer, Kitt Peak National Observatory, National Optical Astronomy Observatory, which is operated by the Association of Universities for Research in Astronomy, Inc. (AURA) under cooperative agreement with the National Science Foundation.

³Visiting Astronomer, Cerro Tololo Inter-American Observatory, National Optical Astronomy Observatory, which is operated by the Association of Universities for Research in Astronomy, Inc. (AURA) under cooperative agreement with the National Science Foundation.

⁴Kitt Peak National Observatory, National Optical Astronomy Observatory, which is operated by the Association of Universities for Research in Astronomy, Inc. (AURA) under cooperative agreement with the National Science Foundation.

same broad-band colors as the cool white dwarfs. This technique is not selective enough to efficiently feed single-object spectrographs. We present the white dwarf cooling sequence using this filter. Our observations show that very cool white dwarfs form a sequence in the $r - DDO$ vs. $r - z$ color-color diagram and demonstrate that significant improvements are needed in white dwarf model atmospheres.

Subject headings: stars: evolution—white dwarfs

1. Introduction

White dwarf stars, remnants of the earliest and all subsequent generations of star formation, are tracers of the age and evolution of the Galaxy. They are initially hot and consequently cool rapidly, though the cooling rate slows as their temperature drops, allowing the oldest white dwarfs to remain visible. Because the cooling rate slows, any census finds more and more white dwarfs at lower and lower temperatures (and luminosities) until, quite abruptly, we find no more of them. Such a census is called the white dwarf luminosity function. Attempts to exploit the white dwarfs as chronometers showed that the white dwarf luminosity function was a map of the history of star formation in the disk, and that there was a shortfall of low luminosity white dwarfs – the inevitable consequence of the finite age of the disk (Liebert 1979; Winget et al. 1987; Liebert, Dahn & Monet 1988).

The cool end of the white dwarf luminosity function was estimated from 43 objects found in the Luyten Half Second Proper Motion Survey (Luyten 1979; Liebert, Dahn & Monet 1988). Proper motion surveys are the most common method of searching for white dwarfs. Since the white dwarfs are intrinsically faint, they must be close to be seen; therefore they tend to have higher proper motions than most other stars with similar magnitudes. Proper motion surveys cannot detect white dwarfs with small tangential velocities, however. Therefore they have complicated and hard to quantify completeness problems. Wood & Oswalt (1998) argue that the ages inferred from the Liebert, Dahn & Monet (1988) white dwarf luminosity function must be considered uncertain by 15% from sampling statistics alone. More importantly, depending on how the data are binned, as many as 3 or as few as 1 of the 43 objects occupy the last bin in the white dwarf luminosity function, precisely

¹Based on observations obtained with the Hobby-Eberly Telescope, which is a joint project of the University of Texas at Austin, the Pennsylvania State University, Stanford University, Ludwig-Maximilians-Universität München, and Georg-August-Universität Göttingen.

the point where all of the age leverage resides. A recent sample of white dwarfs in wide binaries (Oswalt et al. 1996) shows a somewhat lower luminosity downturn which, at the 2σ level, is consistent with no downturn at all in the coolest bin. The simple fact is the fainter age-dependent end of the white dwarf luminosity function is not yet satisfactorily constrained by observation or theory.

An investigation of the cool end of the white dwarf luminosity function that is focused on disentangling theoretical uncertainties in the cooling process would greatly benefit from a much larger kinematically unbiased sample of cool white dwarfs. The details of the constituent input physics can affect the implied ages of white dwarfs below $\log(L/L_\odot) \sim -4.2$ by as much as 2–3 Gyr, hence are critical for using white dwarfs as chronometers (Hawkins & Hambly 1999; Montgomery et al. 1999; Salaris et al. 2000).

A magnitude-limited, kinematically-unbiased sample of white dwarfs can be obtained through a photometric survey. A unique color signature is necessary to photometrically identify a white dwarf among the many other field stars. The magnitude limit of a survey is also a critical factor in the search for cool white dwarfs; if the survey cannot provide sufficiently high signal to noise ratio data for $M_V \sim 16$, it cannot recognize cool low luminosity white dwarfs. Broad-band photometric surveys can be used to find hot white dwarfs due to their blue colors. Recently, Kleinman et al. (2004) found 2551 new white dwarfs with $T_{\text{eff}} \geq 8000$ K in the Sloan Digital Sky Survey Data Release 1. Unfortunately, the broad-band colors of cool white dwarfs are identical to the metal poor subdwarfs. The lack of discovery of cool white dwarfs in the Sloan Digital Sky Survey emphasizes the fact that cool white dwarfs are indistinguishable from subdwarfs and main sequence stars in broad-band photometric observations (e.g. Claver 1995).

In this paper, we investigate the use of the narrow-band DDO51 filter for photometric identification of cool white dwarfs. We present imaging data and follow-up spectroscopy of nine cool white dwarf candidates in §2. In §3, our observations of 30 known cool white dwarfs including four ultra cool white dwarfs are discussed. We also show the cooling sequence for these white dwarfs. We discuss the efficiency and possible use of this filter for photometric identification of cool white dwarfs in §4 along with the observed blue turn-off of very cool white dwarfs.

2. Forward Approach: Photometry to Spectroscopy

Broad-band filter photometry has a limited capacity to distinguish metal poor subdwarfs from cool white dwarfs. In the absence of significant line blanketing, both the white

dwarfs and subdwarfs have broad-band colors that closely approximate those of a blackbody. However, by comparing the flux through a magnesium absorption line-centered filter, e.g. DDO51, several authors have suggested that cool white dwarfs could be distinguished from other field stars of similar T_{eff} (Claver 1995; Harris et al. 2001; Kilic et al. 2003). This is because the majority of cool white dwarfs have essentially featureless spectra around 5150 Å, where subdwarfs and main sequence stars show significant absorption from the Mg β triplet and/or MgH. Figure 1 shows a template spectra for a K5V star (Pickles 1998) and a 5000 K blackbody spectrum along with the tracing of the DDO51, r, and z filters. It is clear from this figure that white dwarfs should be distinguishable from the subdwarf stars using the narrow-band DDO51 filter and a combination of broad-band filters. We note that relative to a blackbody, the K star spectrum deviates both above and below the blackbody line- depending upon the wavelength sampled. Thus, the color indices could just as well be affected by features in the K star beyond 5150 Å as at that wavelength. However, Mg absorption is the strongest feature in the range sampled by the chosen filters, r, z, and DDO51.

In order to test the above claim, Ed Olsewzki kindly provided us with DDO51 photometry of an area of 2 square degrees from the Spaghetti Survey (Morrison et al. 2000) which overlaps with the Sloan Digital Sky Survey fields. A color–color diagram for this field is shown in Figure 2. Two hot white dwarfs found by the Sloan Digital Sky Survey are shown as open circles. Spectroscopically identified QSOs and stars (which are not white dwarfs) are shown as open squares and filled triangles, respectively. Spectral IDs and photometric data for these objects are given in Table 1. A typical errorbar for these objects is shown in the lower left corner of the figure. White dwarfs are expected to be separated from main sequence stars in this color–color diagram (see Figure 4.11 of Claver 1995); we have selected stars that deviate from the main sequence as possible cool white dwarf candidates. Cool white dwarf candidates selected for follow-up spectroscopy at the 9.2m Hobby–Eberly Telescope (HET) and the McDonald 2.7m Harlan–Smith Telescope are shown as filled circles (see Table 2 for photometric information).

2.1. Observations

Follow-up spectroscopy of 9 white dwarf candidates in the Spaghetti Survey Field was obtained in April and May 2002 using the HET and in February 2003 using the 2.7m Harlan–Smith Telescope. We used the HET equipped with the Marcario Low Resolution Spectrograph (LRS) to obtain low resolution spectroscopy of four cool white dwarf candidates. Grism 1 with a 2" slit produced spectra with a resolution of 16 Å over the range 4000 – 10000 Å. Spectroscopy for four additional stars was obtained at the McDonald 2.7m Telescope with

the Imaging Grism Instrument (IGI) and TK4 camera using the holographic grating, which produced spectra with a resolution of 12 Å over the range 4000 – 8000 Å. A spectrophotometric standard star was observed each night for flux calibration. Ne–Cd calibration lamp exposures were taken after each observation with the HET, and Ne–Ar lamp calibrations were taken at the beginning of the night for the 2.7m observations. The data were reduced using standard IRAF² routines.

2.2. Results

The observed spectra for selected white dwarf candidates from the HET and the 2.7m and the fitted template spectra (shown in red) are shown in Figure 3a and 3b, respectively. Spectra are ordered by $g - r$ color. We have used Pickles (1998) template spectra to classify the observed spectra qualitatively. The object numbers, coordinates and the assigned spectral classifications are shown on the lower right corner of the figures. Two of the objects observed at the HET, SDSS J114149.41–001140.4 and SDSS J120709.16–011247.2, show blue excesses. SDSS J114149.41–001140.4 also shows strong H_β and H_γ lines. Therefore we classify these stars as white dwarf + late type star spectroscopic binaries. Figure 3a and 3b show that none of the observed white dwarf candidates are actually single white dwarfs. This discovery contradicted the expected yield of the DDO51 filter which led us to reconsider our strategy for using this filter. We then pursued a reverse approach which is described in the next section.

3. Reverse Approach: Spectroscopy to Photometry

Follow-up spectroscopy of photometrically selected cool white dwarf candidates resulted in the discovery of subdwarf stars and unusual binaries instead of cool white dwarfs. In order to test the effectiveness of the filter in distinguishing cool white dwarfs from subdwarf stars, we decided to observe known cool white dwarfs with the DDO51 filter.

²IRAF is distributed by the National Optical Astronomy Observatory, which is operated by the Association of Universities for Research in Astronomy (AURA), Inc., under cooperative agreement with the National Science Foundation.

3.1. Observations and Results

DDO51, r, and z band photometry of 30 known cool white dwarfs with temperatures ranging from 10000 K down to very cool temperatures ($T_{\text{eff}} \leq 3500$ K) was obtained at the CTIO 4m–Blanco Telescope and Kitt Peak 4m–Mayall Telescope equipped with the $8k \times 8k$ MOSAIC Imager in November 2002 and June 2003, respectively. The MOSAIC Imager when used with these 4m telescopes provides a $35' \times 35'$ field of view. The CCD images were processed with the standard procedures in the MSCRED package in IRAF v2.12. We adopted the reduction procedures used by the NOAO Deep Wide–Field Survey Team³. Images were bias subtracted and flat–fielded using dome flats and sky flats. The z band images were corrected for fringing using the fringing templates derived from the sky flats. We matched star positions in the fields with positions from the USNO–A V2.0 Catalog (Monet et al. 1998) to obtain a plate solution for each CCD. The RMS differences between observed source positions and the USNO–A V2.0 Catalog were less than 0.4 arcseconds. Using the derived astrometric solutions, images were projected to the same uniform (linear, 0.258 arcsecond per pixel) scale.

Source identifications were performed on the projected images using the SExtractor package (Bertin & Arnouts 1996) v2.1.6. The main motivation for using the SExtractor package was its morphological classification. SExtractor uses a neural network to classify objects as stars (stellarity=1) or galaxies (stellarity=0). Stellarity is a continuous variable that can take any value from 0 to 1. A comparison of stellarity indices with magnitudes show that objects with stellarity index ≥ 0.8 have reliable classification as stars. We tested the SExtractor and the IRAF routines WPHOT and PHOT to perform photometry on our images. WPHOT with a gaussian weighting scheme gave the best results for fainter objects, therefore we adopted WPHOT photometry. We selected all objects with a stellarity index larger than 0.8 and with photometric errors less than 0.1 mag for our analysis. Only those objects detected in each filter that matched up to within 0.5 arcsec or better in each coordinate are included in our final catalogs.

Most of our observations were obtained under photometric conditions. Since we are mainly interested in the differential photometry between white dwarfs and the rest of the field stars, data from non–photometric nights are also useful. We have cross-correlated color–color diagrams for each field with the data from the Spaghetti Survey and matched the observed field star sequences to remove any photometric offsets from non–photometric observing conditions. Figure 4 shows the color–color diagram for 30 known white dwarfs and surrounding field stars. Field stars from the Spaghetti Survey and our study are shown

³MOSAIC reduction procedures can be found at <http://www.noao.edu/noao/noaodeep/ReductionOpt/frames.html>

as black dots. A typical errorbar for the field stars is shown in the lower left corner of the figure. A good match between our data and the Spaghetti Survey data is apparent in this figure. Known white dwarfs are shown as filled circles. Our synthetic photometry of white dwarf model atmospheres (Saumon & Jacobson 1999; D. Saumon, private communication) for pure H (solid line) and pure He (dashed line) white dwarfs with $7000 \gtrsim T_{\text{eff}} \gtrsim 3000$ K and a blackbody (dotted line) are also shown. Dashed-dotted lines represent mixed H/He atmospheres for 3500 K and 3000 K white dwarfs with different compositions ($\log [N(\text{He})/N(\text{H})] = -1$ through 6).

Temperatures and colors for the observed white dwarfs are given in Table 3. The observed white dwarf sequence is in agreement with our follow-up spectroscopy, and both demonstrate that white dwarfs are much closer to (and more blended with) the main sequence stars than previously predicted. Cool white dwarfs occupy a region running from the center of the field star locus ($r - DDO = -0.1$, $r - z = 0.05$) for $T_{\text{eff}} \sim 7000$ K to the red edge of the field star locus ($r - DDO = -0.75$, $r - z = 0.65$).

4. Discussion

Our observations demonstrate that the narrow-band DDO51 filter, centered on the Mg band, is not as effective at separating white dwarfs from subdwarfs as we expected. White dwarfs with temperatures between 7000 K and 5000 K ($-0.10 \geq r - DDO \geq -0.45$, $0.05 \leq r - z \leq 0.35$) are photometrically indistinguishable from observed field stars. Using template spectra from the Pickles (1998) library, we have measured the equivalent width of the Mg/MgH feature in main sequence stars. Mg absorption becomes strong enough to affect the photometry in K0 ($T_{\text{eff}} \sim 5000$ K) and later type stars (see Figure 5). Due to the spread in colors and weak Mg absorption in the F–G type stars, white dwarfs with $7000 \text{ K} \geq T_{\text{eff}} \geq 5000$ K have similar colors to F–G stars.

White dwarfs with temperatures in the range 5000–3500 K ($-0.45 \geq r - DDO \geq -0.80$, $0.35 \leq r - z \leq 0.65$) lie just above the edge of the observed field star sequence. Until recently, cool white dwarfs were thought to have spectral energy distributions similar to blackbodies. In fact, this is why Claver (1995) suggested that a narrow-band filter centered on the MgH feature would place cool white dwarfs above the observed field star sequence; the DDO51 filter would separate blackbodies from subdwarfs (see Figure 1 and Figure 4). Although subdwarfs have strong MgH absorption in this temperature range (Figure 5) and they deviate from blackbodies, observed white dwarfs deviate from blackbodies, too. The effects of collision induced absorption (CIA) due to molecular hydrogen are expected to be significant below 5000 K (Hansen et al. 1998; Saumon & Jacobson 1999). Figure 4 shows

that in these colors, there are no pure H white dwarfs with $T_{\text{eff}} \leq 5000$ K and the observed white dwarf sequence actually continues along between the pure H and the pure He models. This is also seen in the $B - V$ vs. $V - K$ color–color diagrams of Bergeron, Ruiz & Leggett (1997) and Bergeron, Leggett & Ruiz (2001) which implies that either all cool white dwarfs have mixed H/He composition, the calculated CIA opacities are incorrect, or there are other neglected physical effects. We note that Bergeron & Leggett (2002) found that all white dwarfs cooler than 4000 K have mixed H/He atmospheres. Even if the white dwarf model atmospheres and the CIA opacities are right, the question of why we still have not found a pure H white dwarf that shows CIA remains to be answered. A possible explanation for the lack of discovery of such objects may simply be the finite age of the Galactic disk; pure H white dwarfs have not yet cooled enough to show strong CIA absorption.

The effective temperature range between 5000 and 3500 K is the most important regime for white dwarf luminosity function studies since it defines the turn–off of the white dwarf luminosity function, hence the age of the observed population. A single slit spectrograph would not be efficient in finding those objects preselected by the DDO51 photometry technique, but a wide field multi–object spectrograph, e.g. Hectospec (Fabricant, Hertz, & Szentgyorgyi 1994) with 300 fibers on the converted Multiple Mirror Telescope, might be used productively to carve out regions from the $r - DDO51$ vs. $r - z$ color–color diagram to find cool white dwarfs in this range. Figure 4 shows a possible search box (shown in green) for cool white dwarfs. For a one square degree field at a Galactic latitude $l = 38$, the box includes 234 stars down to $r = 21.5$. Using the Liebert, Dahn & Monet (1988) white dwarf luminosity function and a disk scale height of 250 pc, we expect to find one cool white dwarf per square degree in the search box ($5000 \text{ K} \geq T_{\text{eff}} \geq 3500 \text{ K}$). In other words, the average pointing with the MMT + Hectospec should yield a cool white dwarf. The above field has 660 stars in the color range $-0.80 \leq r - DDO \leq -0.45$ and 1014 stars in the range $0.35 \geq r - z \geq 0.65$. Even though the DDO51 filter technique is not as efficient as expected, it rejects at least 65% of main sequence stars in this temperature range. Therefore, it is ~ 3 times more efficient than purely spectroscopic (i.e. no prior photometry) surveys. The DDO51 filter is widely used to identify halo stars and to distinguish between giants and dwarfs (Morrison et al. 2001). Thus, as a byproduct, DDO51 photometry from the Spaghetti Survey and similar surveys can be used to identify cool white dwarf candidates for follow-up spectroscopy.

Four ultra cool white dwarfs (CE51, LHS3250, SDSS J133739.40+000142, and LHS1402) lie to the left of the field stars and are clearly separated from the observed sequence of stars due to their depressed near–infrared colors which is thought to be the result of CIA absorption. DDO51 filter photometry is not necessary for finding ultra cool white dwarfs since these stars have broad molecular features and they can be found using broad-band photometry, e.g. in the Sloan Digital Sky Survey. On the other hand, it can help identify the

elusive He-rich ultra cool white dwarfs because they approximate a blackbody spectral energy distribution. The four ultra cool white dwarfs in Figure 4 appear to form a sequence. Ruiz & Bergeron (2001) find an H-dominated atmosphere solution with a temperature estimate of 2730 K for CE51, though infrared photometry is needed to determine the temperature of this star reliably. Simply based on Figure 4, CE51 is more readily explained as a ~ 3200 K white dwarf of mixed composition. Bergeron & Leggett (2002) tried to fit the spectra for LHS3250 and SDSS J133739.40+000142, and found that they are inconsistent with being pure H atmosphere stars. Mixed H/He atmosphere composition is predicted by Bergeron & Leggett (2002), yet the overall shape of the spectra cannot be fitted with the current model atmospheres. Farihi (2004) has found yet another cool white dwarf, GD392B, consistent with a mixed H/He atmosphere. Estimated tangential velocities for the four ultra cool white dwarfs and GD392B are consistent with them being disk objects and their excess luminosity may be explained if they are low-mass white dwarfs or unusual spectroscopic binaries (Ruiz & Bergeron 2001; Harris et al. 2001; Bergeron 2003; Farihi 2004).

Mixed atmosphere white dwarfs cool faster than their pure-H counterparts, therefore they are not the defining stars for the age estimates for the Galactic disk, unless no pure-H atmosphere white dwarfs exist below 4000 K. Although the four ultra cool white dwarfs appear to form a sequence in the $r - DDO51$ vs. $r - z$ color-color diagram, we do not understand their nature at this time. Also, they are not on the theoretically predicted blue hook for cool hydrogen-rich white dwarfs. Our observations demonstrate that optical colors should not be used to estimate the temperatures and ages of ultra cool white dwarfs since current model atmospheres are not fully capable of explaining their observed colors.

Mg/MgH and $CaH + TiO$ are the most prominent features in the optical spectra of subdwarf stars. In addition to the DDO51 filter, we have also investigated the use of an intermediate-band filter centered on the $CaH + TiO$ band at $\sim 6850\text{\AA}$ (Claver 1995) to test whether it can be used to identify white dwarfs. Equivalent width measurements of this band using the Pickles (1998) template spectra are shown in Figure 5. $CaH + TiO$ absorption becomes strong in M0 and later type stars. White dwarfs in this temperature range show depressed infrared colors due to CIA if they have pure-H or mixed H/He atmospheres, and they can be identified by using the DDO51 filter if they have pure-He atmospheres (true-blackbody). The CIA exhibited by ultra cool white dwarfs is extremely broad-band and monotonically varies throughout the red-infrared region, whereas the CaH/TiO band is very narrowly confined in wavelength. Thus, the $CaH + TiO$ filter, if ratioed with another nearby pseudocontinuum filter, could show a much stronger dependency on temperature and metallicity in main sequence and subdwarf stars than it does in ultra cool white dwarfs. Therefore, the $CaH + TiO$ filter and/or JHK infrared photometry may be useful for the identification of cool hydrogen-rich or mixed atmosphere white dwarfs, though broad-band

photometry surveys are also successful in finding ultra cool white dwarfs (e.g. Sloan Digital Sky Survey; Harris et al. 2001; Gates et al. 2004).

We thank Jennifer Claver for useful discussions on reducing MOSAIC data and the NOAO Deep Wide-Field Survey Team for making their reduction procedures available online. We also thank Didier Saumon for making his cool white dwarf model atmospheres available to us and for careful reading of this manuscript. We are grateful to Ed Olsewzki for making his DDO51 photometry data available to us. This material is based upon work supported by the National Science Foundation under Grant No. 0307315. The Hobby-Eberly Telescope (HET) is a joint project of the University of Texas at Austin, the Pennsylvania State University, Stanford University, Ludwig-Maximilians-Universität München, and Georg-August-Universität Göttingen. The HET is named in honor of its principal benefactors, William P. Hobby and Robert E. Eberly. The Marcario Low Resolution Spectrograph is named for Mike Marcario of High Lonesome Optics who fabricated several optics for the instrument but died before its completion. The LRS is a joint project of the Hobby-Eberly Telescope partnership and the Instituto de Astronomia de la Universidad Nacional Autonoma de México.

REFERENCES

Bergeron, P., Ruiz, M. T. & Leggett, S. K. 1997, *ApJS*, 108, 339

Bergeron, P., Leggett, S. K. & Ruiz, M. T. 2001, *ApJS*, 133, 413

Bergeron, P. & Leggett, S. K. 2002, *ApJ*, 580, 1070

Bergeron, P. 2003, *ApJ*, 586, 201

Bertin, E. & Arnouts, S. 1996, *A&AS*, 117, 393

Chabrier, G. Segretain, L., Hernanaz, M., & Mochkovitch, R., 1993, in The VIII European Workshop on White Dwarfs, ed. M. A. Barstow (Dordrecht: Kluwer), 115

Claver, C. F. 1995, Ph.D. Thesis, University of Texas

De Marchi, G., Paresce, F., Straniero, O., and Prada Moroni, P.G. 2004, *A&A*, in press

Fabricant, D. G., Hertz, E. H. & Szentgyorgyi, A. H. 1994, Proc. SPIE Vol. 2198, p. 251-263, Instrumentation in Astronomy VIII, David L. Crawford; Eric R. Craine; Eds

Farihi, J. 2004, ApJ, in press

Fontaine, G., Brassard, P., & Bergeron, P. 2001, PASP, 113, 409

Gates, E. et al. 2004, preprint, astro-ph/0405566

Hansen, B. M. S. 1998, 19th Texas Symposium on Relativistic Astrophysics and Cosmology, held in Paris, France, Dec. 14-18, 1998. Eds, p. 283

Harris, H. C. et al. 2001, ApJ, 549, 109

Kilic, M., Winget, D.E., von Hippel, T., & Claver, C.F. 2003, in The XIII European Workshop on White Dwarfs, ed. D. de Martino, R. Silvotti, J.-E. Solheim, & R. Kalytis (Dordrecht: Kluwer), 389

Kleinman, S. J. et al. 2004, in press

Knox, R. A., Hawkins, M. R. S., & Hambly, N. C. 1999, MNRAS, 306, 736

Leggett, S. K., Ruiz, M. T., & Bergeron, P. 1998, ApJ, 497, 294

Liebert, J. 1979, In IAU Colloquium 53: White Dwarfs and Variable Degenerate Stars, p. 146

Liebert, J., Dahn, C. C., & Monet, D. G. 1988, ApJ, 332, 891

Monet, D. B. A. et al. 1998, VizieR Online Data Catalog, October, 1252

Montgomery, M. H., Klumpe, E. W., Winget, D. E., & Wood, M. A. 1999, ApJ, 525, 482

Morrison, H. L. et al. 2000, AJ, 119, 2254

Oppenheimer, B. R. Hambly, N. C. Digby, A. P. Hodgkin, S. T. & Saumon, D. 2001, Science, 292, 698

Oswalt, T. D., Smith, J. A., Wood, M. A., & Hintzen, P. M. 1996, Nature, 382, 692

Pickles, A. J. 1998, PASP 110, 863

Ruiz, M. T. & Bergeron, P. 2001, ApJ, 558, 761

Salaris, M., García-Berro, E., Hernanz, M., Isern, J., & Saumon, D. 2000, ApJ, 544, 1036

Saumon, D. & Jacobson, S. B. 1999, ApJ, 511, 107

Wesemael, F. et al. 1993, PASP, 105 ,761

Winget, D. E., Hansen, C. J., Liebert, J., Van Horn, H. M., Fontaine, G., Nather, R. E., Kepler, S. O., & Lamb, D. Q. 1987, *ApJ*, 315, L77

Wood, M. A. 1995, in *The IX European Workshop on White Dwarfs*, ed. Detlev Koester & Klaus Werner (Berlin: Springer), 41

Table 1. Objects with SDSS Spectroscopy

Object	Plate	MJD	Fiber	ddo	u	g	r	i	z	σ_{ddo}	σ_u	σ_g	σ_r	σ_i	σ_z	Type
SDSS J101748.90-003124.5	271	51883	166	18.68	19.30	18.86	18.84	18.85	18.65	0.01	0.03	0.01	0.01	0.01	0.03	QSO
SDSS J101807.04-002003.3	271	51883	174	20.14	20.99	19.98	19.91	19.97	19.49	0.02	0.12	0.02	0.03	0.04	0.08	QSO
SDSS J101741.70-002934.1	271	51883	181	16.34	16.56	16.28	16.72	16.88	17.17	0.01	0.01	0.01	0.01	0.01	0.02	WD
SDSS J101651.74-003347.0	271	51883	226	19.14	18.93	19.01	18.95	18.65	18.64	0.01	0.02	0.02	0.01	0.01	0.04	QSO
SDSS J105907.68+010303.5	277	51908	361	19.26	19.20	19.17	18.88	18.78	18.83	0.01	0.03	0.01	0.02	0.02	0.04	QSO
SDSS J105934.61+011112.1	277	51908	377	17.81	18.82	17.86	17.50	17.38	17.34	0.01	0.02	0.01	0.03	0.01	0.02	Star
SDSS J110015.66+010740.5	277	51908	414	18.80	19.09	18.74	18.99	19.30	19.57	0.01	0.02	0.01	0.02	0.03	0.08	WD
SDSS J110010.68+010328.3	277	51908	416	16.89	18.97	17.63	17.40	17.31	17.30	0.01	0.02	0.01	0.02	0.02	0.02	Star
SDSS J112941.64+000545.3	281	51614	117	18.60	19.63	18.61	18.57	18.53	18.61	0.01	0.04	0.02	0.02	0.03	0.06	Star
SDSS J112837.56-000112.6	281	51614	142	19.05	19.57	18.35	18.32	18.38	18.34	0.01	0.03	0.01	0.01	0.01	0.03	Star
SDSS J112839.72+002644.3	281	51614	485	18.11	19.35	18.19	17.98	17.99	18.01	0.01	0.04	0.03	0.01	0.02	0.03	Star
SDSS J113015.48+002843.9	281	51614	551	17.74	17.71	17.68	17.72	17.93	17.90	0.01	0.01	0.02	0.02	0.02	0.02	QSO
SDSS J113026.84+002649.1	282	51658	348	20.20	20.01	19.99	20.09	19.83	19.77	0.02	0.05	0.03	0.03	0.04	0.11	QSO
SDSS J113031.57+002033.4	282	51658	353	17.95	18.08	18.04	17.87	17.88	17.84	0.01	0.01	0.02	0.01	0.02	0.02	QSO
SDSS J113003.26+000332.4	282	51658	356	19.63	19.64	19.53	19.55	19.37	19.23	0.01	0.04	0.02	0.03	0.04	0.09	QSO
SDSS J113009.77+001737.6	282	51658	357	19.70	20.89	19.81	19.80	19.40	19.36	0.02	0.06	0.03	0.03	0.02	0.06	Star
SDSS J114311.23-002133.0	283	51959	224	18.99	18.88	18.92	18.83	18.72	18.56	0.01	0.02	0.02	0.02	0.03	0.04	QSO
SDSS J114321.76-002941.5	283	51959	229	18.81	19.32	19.10	19.11	19.26	18.96	0.01	0.03	0.01	0.02	0.02	0.04	QSO
SDSS J114318.48-002254.9	283	51959	237	18.59	19.57	18.63	18.45	18.46	18.42	0.01	0.03	0.02	0.02	0.03	0.03	Star
SDSS J114210.47-002013.0	283	51959	238	19.08	19.36	19.16	18.89	18.87	18.76	0.01	0.03	0.02	0.03	0.05	0.04	QSO
SDSS J114137.14-002729.8	283	51959	262	18.61	18.94	18.75	18.59	18.42	18.18	0.01	0.02	0.01	0.02	0.01	0.03	QSO
SDSS J114151.31-000729.7	283	51959	398	17.10	18.05	17.17	16.90	16.82	16.81	0.01	0.01	0.01	0.01	0.02	0.02	Star
SDSS J114259.30-000156.5	283	51959	435	19.47	19.96	19.50	19.18	18.93	18.69	0.02	0.04	0.01	0.02	0.02	0.03	QSO
SDSS J120637.75-011246.6	286	51999	81	17.29	18.24	17.34	17.12	17.00	16.98	0.01	0.02	0.01	0.02	0.01	0.02	Star
SDSS J120631.48-010801.8	286	51999	85	19.37	20.38	19.44	19.12	19.02	18.87	0.01	0.07	0.02	0.02	0.03	0.06	Star
SDSS J120708.35-010002.5	286	51999	86	19.07	19.12	19.09	18.94	18.59	18.50	0.01	0.03	0.02	0.01	0.02	0.03	QSO
SDSS J123056.59-005306.4	289	51990	17	18.89	19.26	18.87	18.73	18.72	18.46	0.01	0.03	0.02	0.01	0.01	0.03	QSO
SDSS J123213.28-003106.3	289	51990	25	19.08	20.22	19.07	19.15	19.21	19.28	0.02	0.04	0.02	0.01	0.02	0.05	Star
SDSS J123051.62-004437.1	290	51941	284	18.00	19.00	17.84	17.97	18.03	18.14	0.01	0.02	0.02	0.02	0.02	0.03	Star
SDSS J123149.22-005550.4	290	51941	292	17.49	18.45	17.46	17.43	17.48	17.53	0.01	0.01	0.02	0.01	0.01	0.01	Star
SDSS J123140.81-004435.1	290	51941	293	18.71	19.68	18.75	18.62	18.58	18.56	0.01	0.03	0.02	0.02	0.02	0.04	Star
SDSS J123027.54-003633.3	290	51941	319	16.88	17.84	16.79	17.07	17.29	17.37	0.01	0.01	0.02	0.01	0.02	0.01	Star
SDSS J131941.10-004340.6	296	51984	184	20.46	23.35	20.85	19.27	17.21	16.03	0.03	0.68	0.04	0.02	0.01	0.01	Star
SDSS J131938.76-004940.0	296	51984	189	17.59	17.73	17.54	17.48	17.50	17.40	0.01	0.02	0.02	0.01	0.01	0.02	QSO
SDSS J143143.80-005011.4	306	51637	129	18.05	18.31	18.09	17.85	17.81	17.89	0.01	0.02	0.02	0.02	0.02	0.02	QSO

Table 1—Continued

Object	Plate	MJD	Fiber	ddo	u	g	r	i	z	σ_{ddo}	σ_u	σ_g	σ_r	σ_i	σ_z	Type
SDSS J143158.36–004303.9	306	51637	138	19.14	19.06	18.99	18.80	18.74	18.88	0.01	0.02	0.03	0.02	0.02	0.03	QSO
SDSS J143153.06–002824.3	306	51637	194	17.82	17.29	17.66	18.21	18.91	18.85	0.01	0.02	0.02	0.02	0.03	0.04	SDO
SDSS J143037.11–004748.9	306	51637	255	16.98	17.92	17.02	16.89	16.88	16.89	0.01	0.02	0.01	0.01	0.02	0.01	Star
SDSS J145321.76+010130.6	538	52029	212	19.95	20.53	20.10	20.15	19.96	19.68	0.02	0.06	0.02	0.03	0.04	0.08	QSO
SDSS J145244.19+010954.9	538	52029	251	19.97	20.21	20.21	19.90	19.88	19.56	0.02	0.05	0.03	0.03	0.03	0.08	QSO

Table 2. Objects with HET + McDonald 2.7m Spectroscopy

No	Object	ddo	u	g	r	i	z	σ_{ddo}	σ_u	σ_g	σ_r	σ_i	σ_z
1	SDSS J114149.41–001140.4	19.67	20.49	19.77	19.14	18.05	17.32	0.01	0.05	0.02	0.02	0.02	0.02
2	SDSS J120650.72–010519.1	20.29	22.44	20.81	19.44	17.87	17.11	0.02	0.43	0.06	0.05	0.02	0.03
3	SDSS J120651.91–010435.2	19.31	21.30	19.38	18.59	18.32	18.14	0.01	0.16	0.01	0.02	0.02	0.03
4	SDSS J120709.16–011247.2	16.84	18.12	16.90	16.34	15.70	15.33	0.02	0.01	0.01	0.02	0.01	0.02
5	SDSS J120741.55–010630.9	19.89	22.70	20.07	19.62	18.39	18.17	0.02	1.17	0.15	0.19	0.08	0.09
6	SDSS J123202.54–010232.1	20.33	22.88	20.59	19.25	17.94	17.25	0.04	0.98	0.03	0.02	0.01	0.01
7	SDSS J123208.81–010230.5	20.69	22.52	20.68	19.82	19.37	19.03	0.04	0.31	0.03	0.02	0.02	0.04
8	SDSS J131833.56–004448.4	16.59	18.76	16.80	16.11	15.68	15.41	0.01	0.02	0.02	0.01	0.02	0.01
9	SDSS J143044.16–002853.1	16.99	18.74	17.09	16.53	16.35	16.63	0.01	0.03	0.01	0.01	0.02	0.02

Table 3. DDO51 photometry for previously identified white dwarfs

Object	R	$r - z$	σ_{r-z}	$r - ddo$	σ_{r-ddo}	$T_{\text{eff}}(\text{K})$	Notes
WD2323+157	15.04	-0.31	0.01	0.19	0.01	10170	1
LTT 9491	14.07	-0.37	0.01	0.19	0.01	...	2
CE157	15.64	0.03	0.03	-0.07	0.02	7000	3
WD1325+581	16.42	0.07	0.01	-0.15	0.01	6810	4
WD1633+572	14.68	0.08	0.01	-0.16	0.01	6180	4
WD2107-216	16.45	0.09	0.01	-0.21	0.01	5830	4
WD2347+292	15.41	0.13	0.01	-0.14	0.01	5810	4
WD0752-676	13.58	0.09	0.01	-0.22	0.01	5730	4
CE162	16.69	0.12	0.01	-0.21	0.01	5730	3
WD1257+037	15.46	0.21	0.01	-0.22	0.01	5590	4
WD2248+293	15.14	0.19	0.01	-0.21	0.01	5580	4
WD0121+401	16.67	0.28	0.01	-0.31	0.01	5340	4
WD1334+039	14.12	0.36	0.01	-0.43	0.01	5030	4
WD2002-110	16.36	0.29	0.01	-0.38	0.01	4800	4
WD0045-061	17.70	0.32	0.01	-0.40	0.01	...	5
WD1820+609	15.15	0.37	0.01	-0.45	0.01	4780	4
LHS 542	17.53	0.44	0.04	-0.57	0.01	4720	4
WD1108+207	17.17	0.45	0.01	-0.50	0.01	4650	4
WD1345+238	15.12	0.45	0.01	-0.57	0.01	4590	4
WD2251-070	15.10	0.46	0.01	-0.54	0.01	4580	4
CE40	18.82	0.50	0.01	-0.63	0.01	4580	3
CE142	18.59	0.55	0.02	-0.70	0.02	4390	3
CE16	17.59	0.64	0.01	-0.78	0.01	4330	3
WD1300+263	18.09	0.56	0.01	-0.67	0.01	4320	4
WD1247+550	17.03	0.66	0.01	-0.75	0.01	4050	4
F351-50	18.37	0.56	0.01	-0.80	0.01	3500:	5
CE51	17.50	-0.36	0.01	-0.55	0.01	2730:	3
LHS 3250	17.87	-0.69	0.03	-0.26	0.01	...	6
SDSS J133739.40+000142.8	19.16	-0.82	0.11	-0.20	0.02	...	6
LHS 1402	17.86	-0.96	0.02	0.03	0.01	...	5

Note. — (1) R magnitude and T_{eff} from Bergeron, Ruiz & Leggett 1997; (2) Spectral Type DBQA5 (Wesemael et al. 1993); (3) R magnitude and T_{eff} from Ruiz & Bergeron 2001; (4) R magnitude and T_{eff} from Bergeron, Leggett & Ruiz 2001; (5) R_{59F} magnitude and/or T_{eff} from Oppenheimer et al. 2001; (6) SDSS r magnitude

Fig. 1.— Template spectra for a K5V star (Pickles 1998) and a 5000 K blackbody. The tracing for the DDO51, r, and z filters are shown as dotted-lines. The greatest difference between the blackbody and the template stellar spectra, Mg absorption, is apparent in this figure.

Fig. 2.— $r - DDO51$ vs. $r - z$ color–color diagram of a 2 square degree field from the Spaghetti Survey which overlaps with the Sloan Digital Sky Survey fields. Two hot, spectroscopically identified white dwarfs are shown as open circles. Quasars and stars (which are not white dwarfs) are shown as open squares and filled triangles, respectively. Cool white dwarf candidates selected for follow-up spectroscopy are shown as filled circles. We note that # 3 and #6 were not selected as cool white dwarf candidates, but they happened to be positioned on the slit during our observations of cool white dwarf candidates.

Fig. 3.— Optical spectra for the white dwarf candidates observed at the HET (Figure 3a) and the 2.7m (Figure 3b). Template spectra (Pickles 1998) used to classify these objects are shown in red. Object numbers, coordinates and spectral types are shown in the lower right corner. Note that the feature at 7600 Å is telluric and the emission features in # 1 at \sim 7700 Å and in # 2 at \sim 4300 Å are due to cosmic ray hits.

Fig. 4.— $r - DDO51$ vs. $r - z$ color–color diagram for 30 known white dwarfs (filled circles) and the surrounding field stars (black dots). A typical errorbar for the field stars is shown in the lower left corner. Our synthetic photometry of pure H and pure He white dwarf models with $7000 \gtrsim T_{\text{eff}} \gtrsim 3000$ K are shown as solid and dashed lines, respectively. Dashed-dotted lines represent mixed atmospheres for 3500 K and 3000 K white dwarfs with different compositions and a blackbody is also shown as a dotted line. The green box marks a possible search region for cool white dwarfs.

Fig. 5.— Equivalent width of the Mg/MgH and CaH+TiO features measured from Pickles (1998) template spectra. The Mg/MgH feature becomes strong enough to affect the photometry in K0 and later type stars, whereas the CaH+TiO feature dominates at \sim 6850 Å for M0 and later type stars.

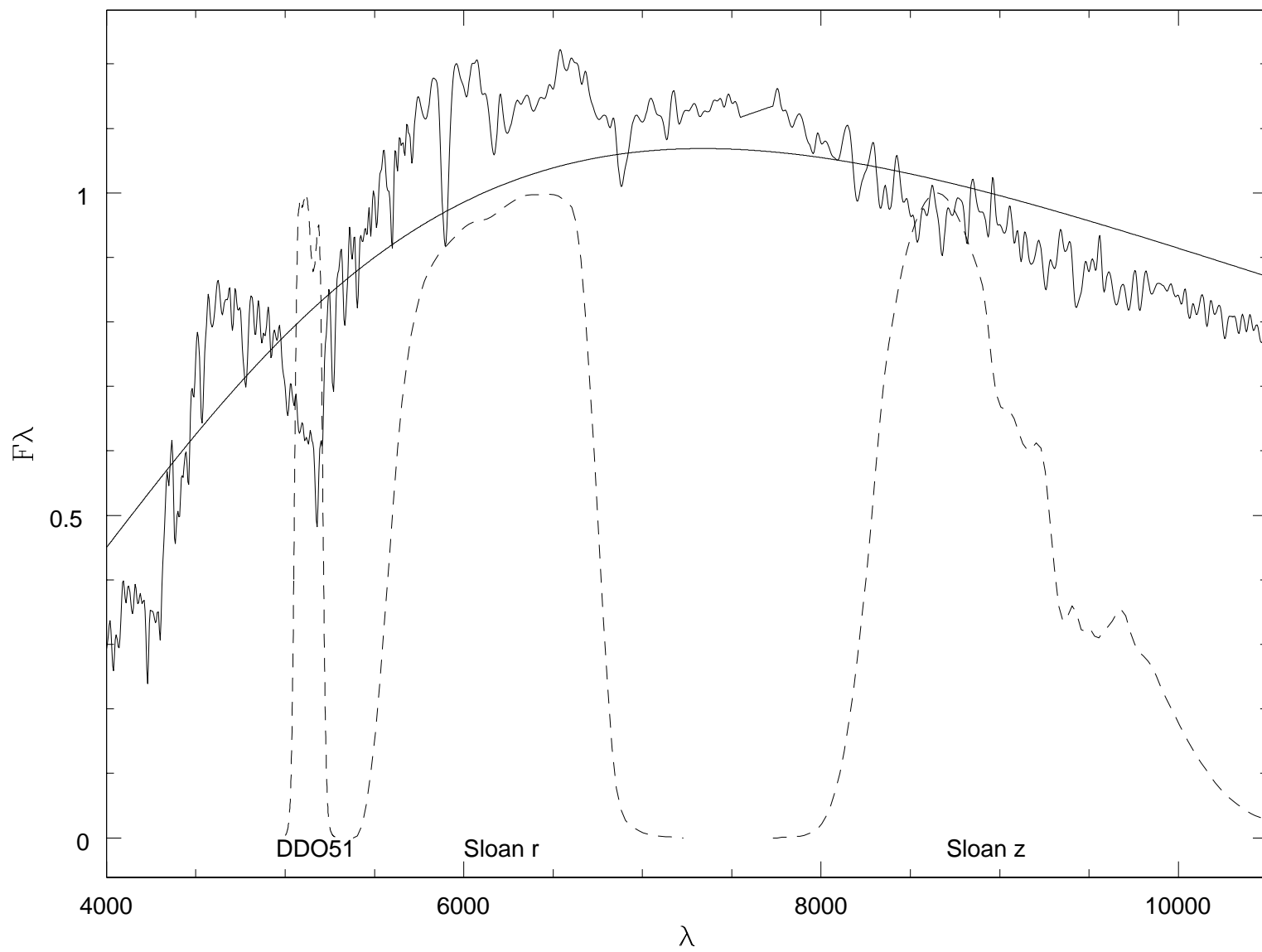


Figure 1

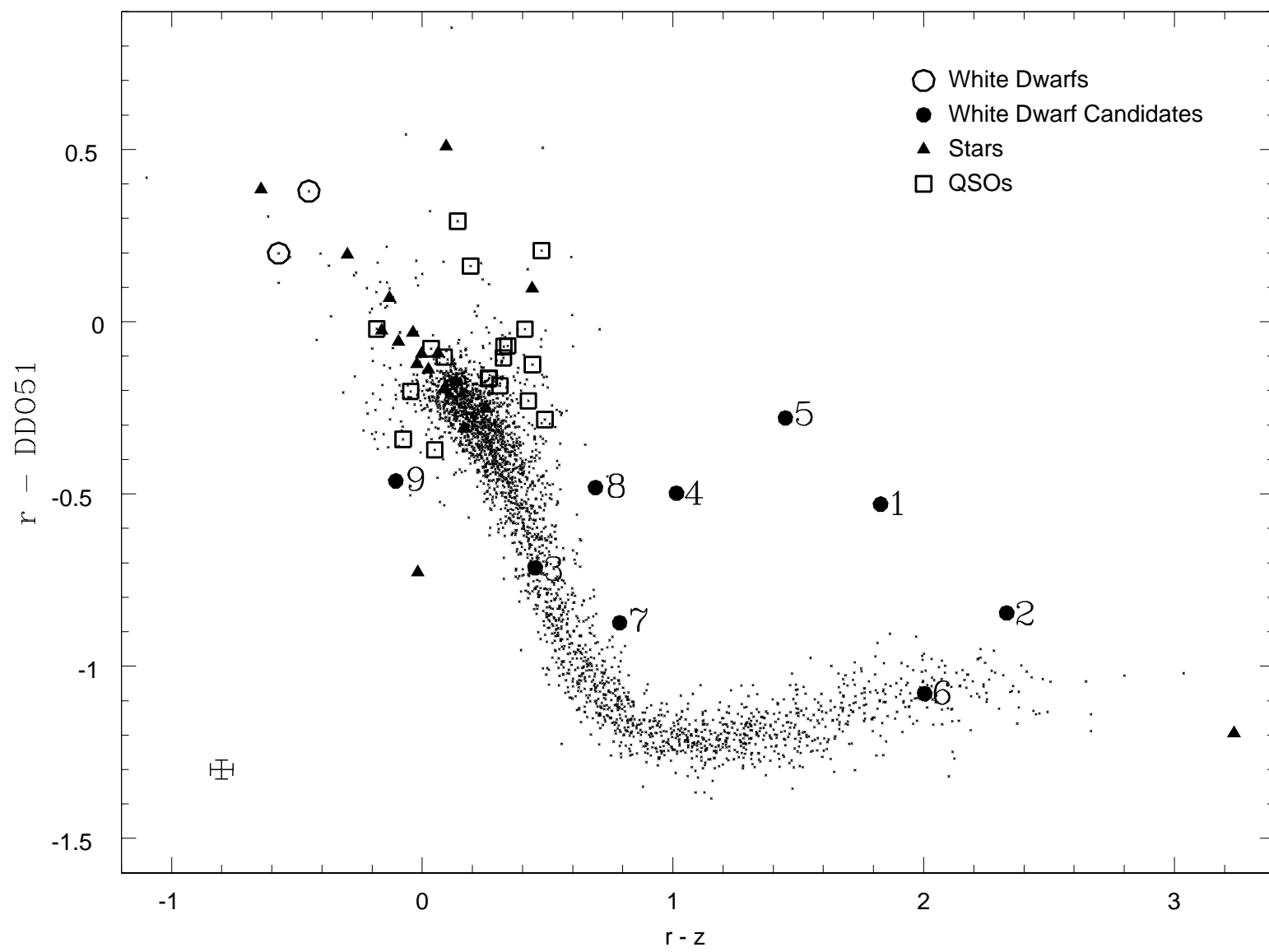


Figure 2

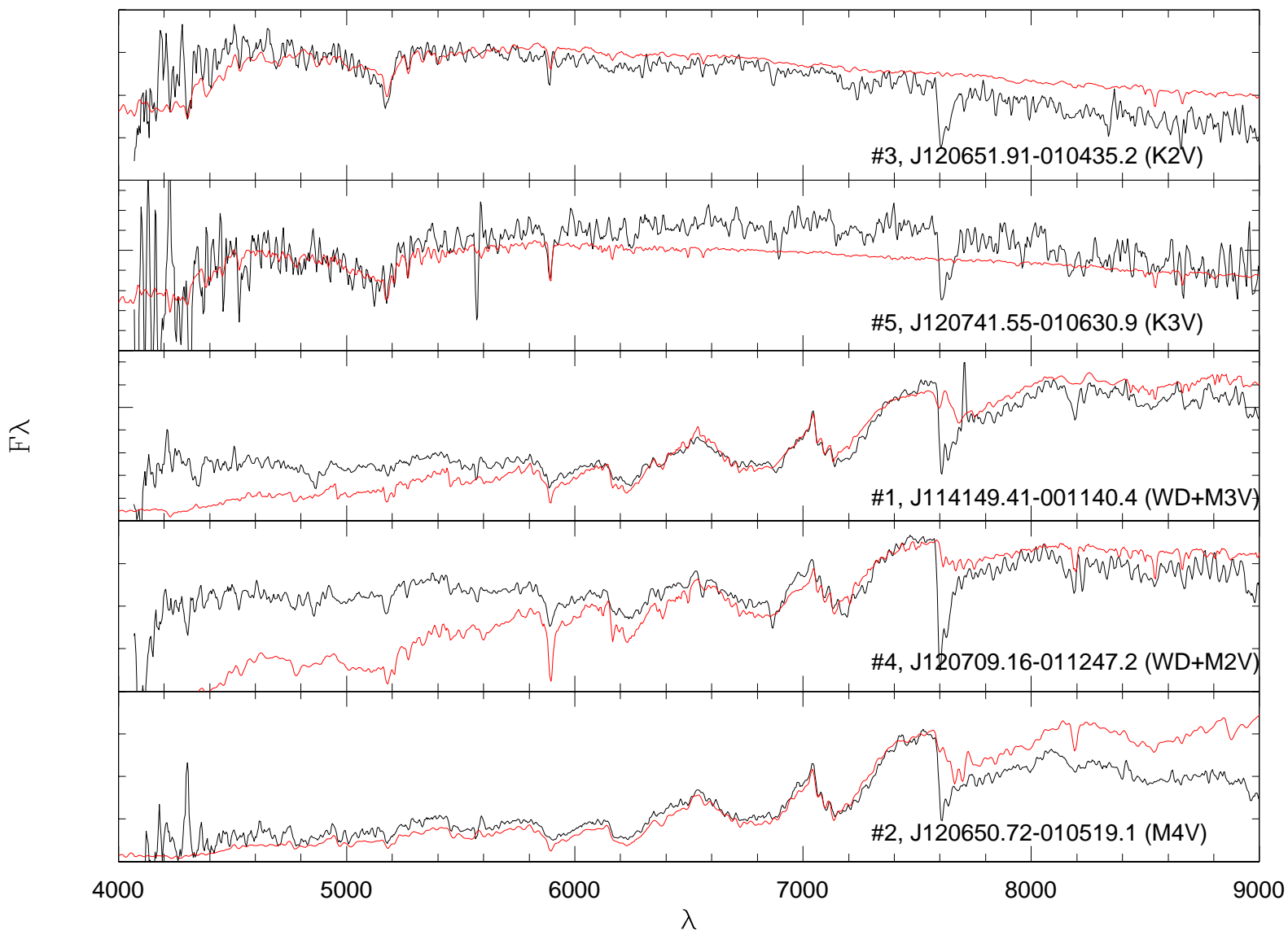


Figure 3a

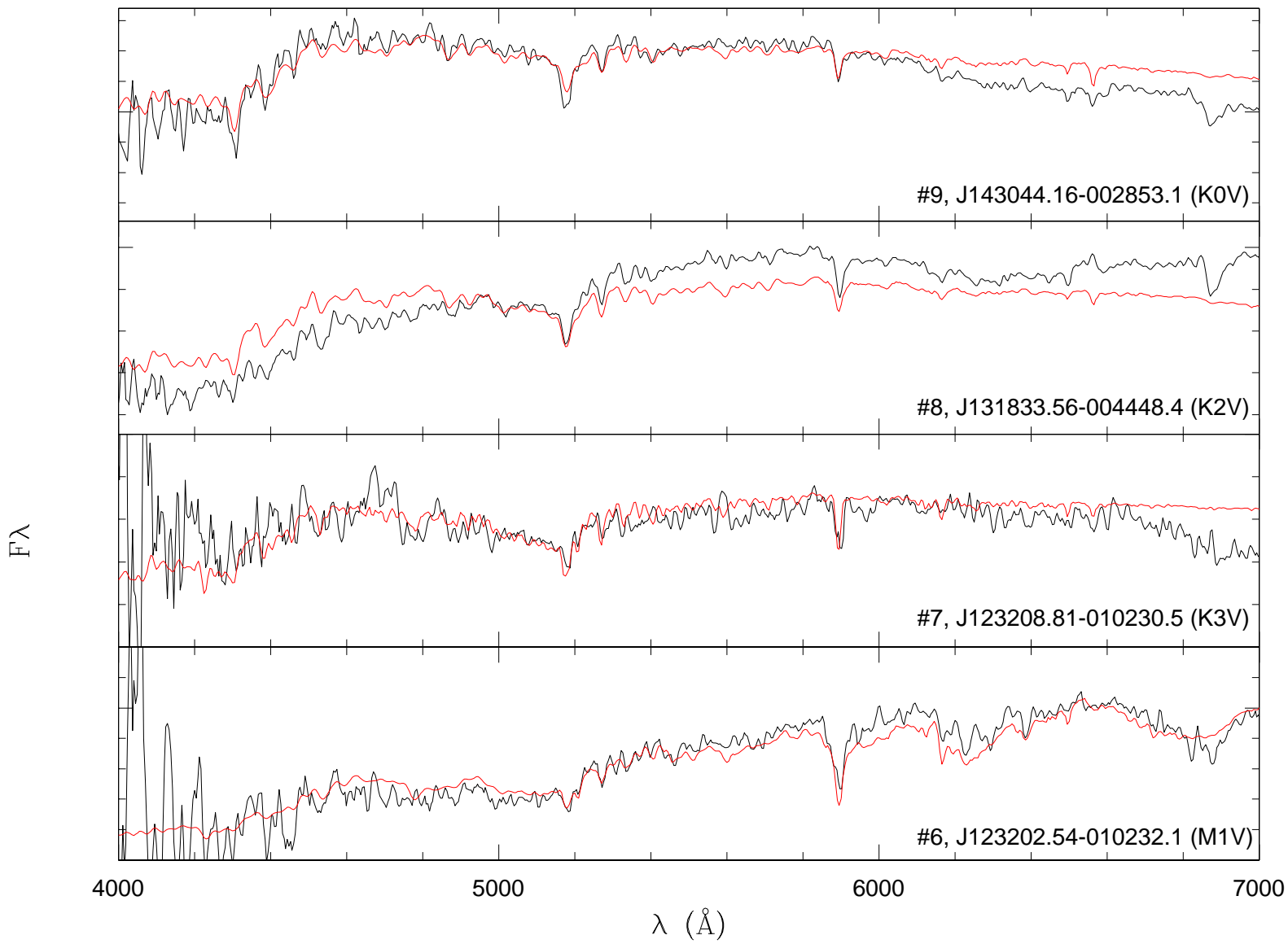


Figure 3b

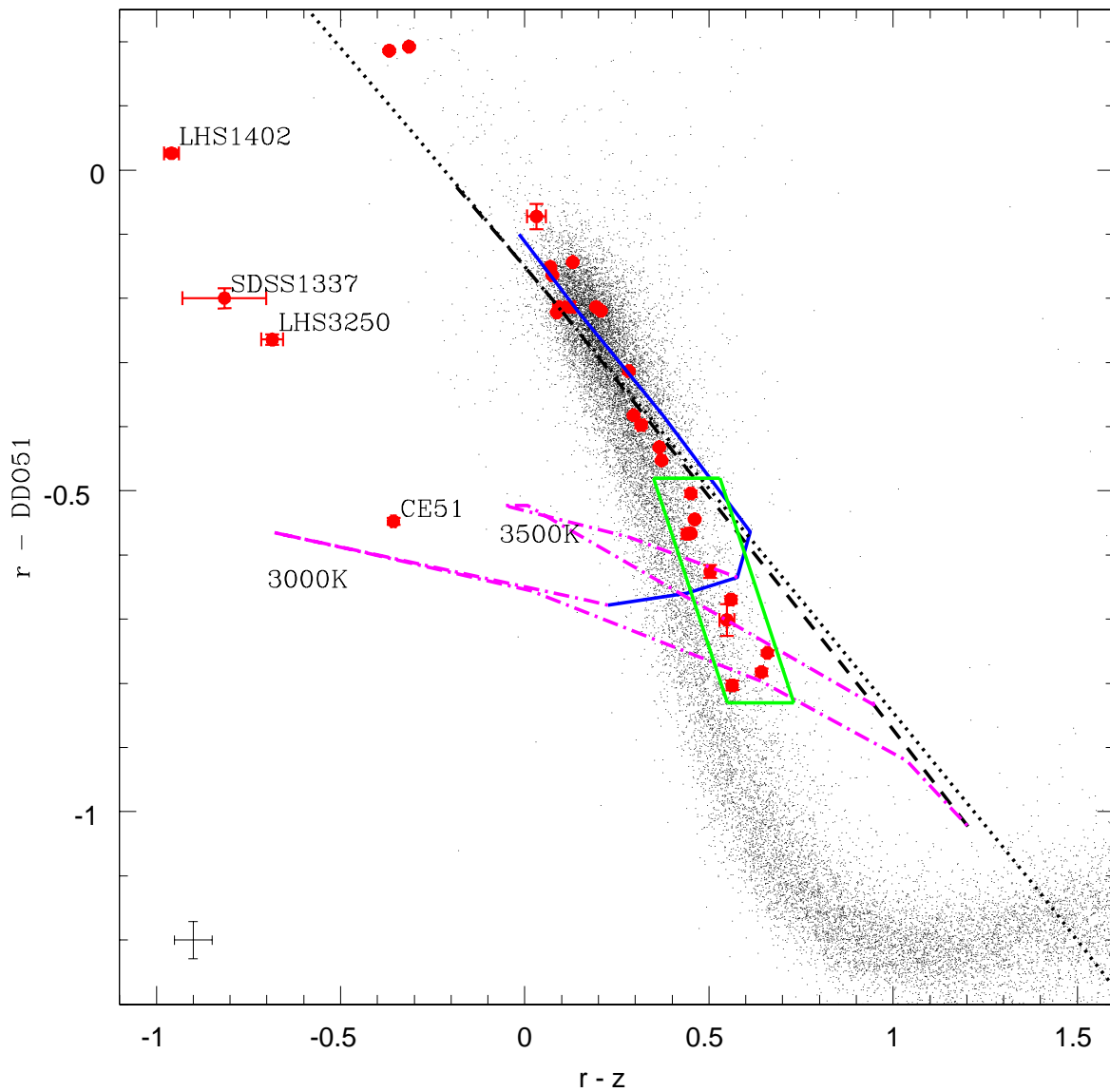


Figure 4

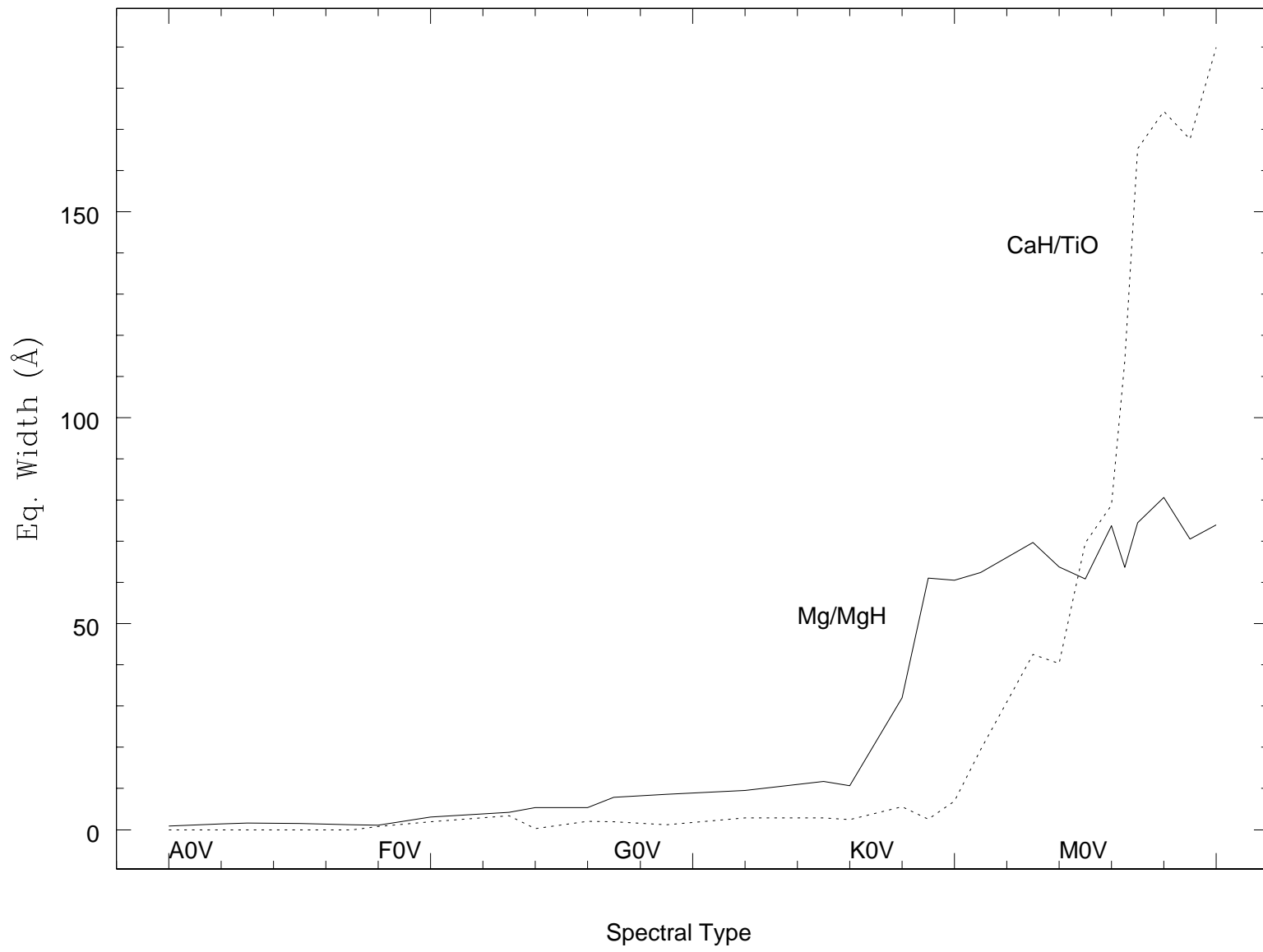


Figure 5